의학박사 학위논문

Characteristics and Mechanisms of Glucose Hypermetabolism in Denervated Skeletal Muscle

탈신경근육에서 포도당대사 증진현상의 특성과 기전

2017년 8월

서울대학교 대학원

의학과 재활의학 전공

이 승 학

ABSTRACT

Characteristics and Mechanisms of Glucose Hypermetabolism in Denervated Skeletal Muscle

Seung Hak Lee

Department of Rehabilitation Medicine,

Seoul National University College of Medicine

Peripheral nerve injury is caused by various etiologies including trauma, leading to denervation of muscles. Muscle denervation is accompanied by extensive molecular changes related to muscle structure, dynamic properties, cell membrane properties, muscle activation processes, etc., over time. Among them, glucose hypermetabolism has been demonstrated through ^{18}F-fluorodeoxyglucose (^{18}F-FDG) positron emission tomography (PET) in animal experiments; moreover, the same phenomenon has been confirmed in humans. The purpose of the present study is to investigate characteristics of glucose hypermetabolism in muscle denervation and explore its molecular mechanisms. Through this, the foundation for clinical applications of this physiological phenomenon can be established.

Sciatic nerves were transected in rats to generate a complete nerve injury model; ^{18}F-FDG PET scans were then taken serially to examine the temporal characteristics of glucose hypermetabolism. We also investigated the correlation between the severity of nerve injury and signal intensity of ^{18}F-FDG uptake in a partial nerve injury model by partially ligating the peroneal division of the sciatic nerve. Western blot analyses were performed to investigate the expression of several important intracellular pathways involved in glucose metabolism. Finally, the effect of the mechanistic target of rapamycin (mTOR) pathway was examined by analyzing the changes in glucose metabolism in the denervated muscles of rats treated with rapamycin, an inhibitor of mTOR.

We calculated the mean lesion-to-normal counts ratio (LNR_{mean}) as an quantitative value of ^{18}F-FDG uptake signal. Our data showed that glucose metabolism in the denervated anterior compartment muscles of the complete injury model significantly increased starting from the second day of nerve injury (LNR_{mean}, sham, 1.332 ± 0.205; LNR_{mean}, denervation, 3.151 ± 0.822; $n = 5$; $P < 0.05$). Increased uptake of ^{18}F-FDG continued for up to 12 weeks (LNR_{mean}, sham, 1.316 ± 0.275; LNR_{mean}, denervation, 2.661 ± 0.749; $n = 5$; $P < 0.05$). In addition, the peak of glucose hypermetabolism appeared 1 week after nerve injury, and was more than seven-fold higher than that of the sham side (LNR_{mean}, sham, 1.360 ± 0.452; LNR_{mean}, denervation, 10.340 ± 4.094; $n = 5$; $P < 0.05$). In the partial injury model, ^{18}F-FDG uptake was lower compared to that in the complete nerve injury model; there was a strong correlation between the quantified nerve injury severity and ^{18}F-FDG uptake signal in the denervated muscle (Pearson's correlation coefficient, 0.63; $P < 0.05$). Western blot analyses of denervated muscles 1 week after complete

nerve injury showed significant increase in the expressions of mTOR (sham, 0.103 ± 0.118; denervation, 0.703 ± 0.466; n = 6; $P < 0.05$), phospho-mTOR (sham, 0.055 ± 0.0232; denervation, 0.981 ± 0.590; n = 6; $P < 0.05$), Bax (sham, 0.358 ± 0.101; denervation, 1.006 ± 0.127; n = 6; $P < 0.05$), and Bcl-2 (sham, 0.862 ± 0.128; denervation, 1.060 ± 0.062; n = 6; $P < 0.05$). PET scans taken 1 week after complete sciatic nerve injury in rats, treated with rapamycin showed increased ^{18}F-FDG uptake in denervated muscle compared to the sham side. However, it was about 40% of the signal intensity of the untreated complete injury model at the same time point. (LNR_{mean}, denervation, rapamycin treated, 4.185 ± 1.253; LNR_{mean}, denervation, rapamycin untrerated, 10.340 ± 4.094; n = 5; $P < 0.05$)

The present study showed that glucose hypermetabolism in the denervated muscle begins at day 2, lasts up to 12 weeks, and is maximal at 1 week after denervation in a rat sciatic transection model. Increased glucose uptake was related to the degree of nerve injury severity. The molecular mechanism of this phenomenon seems to be heterogeneous and multiphasic. The mTOR pathway is thought to play an important role, especially at the time of maximal hypermetabolism. Based on these results, a new functional imaging study can be developed for diagnosis and evaluation of peripheral neuromuscular disorders.

Keywords: peripheral nerve injury, muscle denervation, glucose metabolism. ^{18}F-fluorodeoxyglucose, positron emission tomography, mechanistic target of rapamycin

Student Number: 2013-21688

TABLE OF CONTENTS

Abstract ..... **i**

Table of contents ..... **iv**

List of tables and figures ..... **v**

List of abbreviations ..... **vii**

Introduction **1**

Materials and methods **9**

Results **14**

Discussion **27**

References **35**

국문초록 **42**

LIST OF TABLES

Table 1. Classification System for Peripheral Nerve Injury

Table 2. Advantages and Disadvantages of Current Diagnostic Methods for Peripheral Nerve Injury

LIST OF FIGURES

Figure 1. Serial ^{18}F-fluorodeoxyglucose (^{18}F-FDG) positron emission tomography (PET) scans show temporal characteristics of glucose hypermetabolism in denervated skeletal muscle.

Figure 2. In a partial peroneal injury model, the increase in ^{18}F-FDG uptake is relatively small compared to the increase in ^{18}F-FDG uptake in a complete injury model.

Figure 3. Inflammatory cell infiltration does not increase in the tibialis anterior muscle, one week after denervation.

Figure 4. The results from western blot analyses show significantly higher expressions of proteins related to mTOR and apoptosis pathways in denervated tibialis anterior muscle compared to those in sham side muscle.

Figure 5. ^{18}F-FDG PET scans of the hind limbs in rapamycin treated rats with left

sciatic nerve transection show less increase in ^{18}F-FDG uptake in the denervated muscle compared to the increase in ^{18}F-FDG uptake in untreated rats.

LIST OF ABBREVIATIONS

AMPK	adenosine monophosphate-activated protein kinase
ASA	abnormal spontaneous activities
BSA	bovine serum albumin
CaMK	Ca^{2+}/calmodulin-dependent protein kinase
CMAP	compound motor action potential
EMG	electromyography
FDG	fluorodeoxyglucose
GLUT	glucose transporter
H&E	hematoxylin and eosin
IACUC	Institutional Animal Care and Use Committee
IHC	immunohistochemistry
LNR	lesion-to-normal counts ratio
MRI	magnetic resonance imaging
mTOR	mechanistic target of rapamycin
NCS	nerve conduction study
PET	positron emission tomography
PVDF	polyvinylidene fluoride
RM-ANOVA	repeated-measures analysis of variance
ROIs	regions of interest
TBP	TATA-binding protein
USG	ultrasonography
WB	western blot

INTRODUCTION

Peripheral nerve injury, focused on trauma

The etiology of peripheral nerve injury includes a number of causes, including trauma, ischemia, endocrinologic disorders, and autoimmune disorders. It is known to occur over the general peripheral nervous system or in individual nerve segments (1). The former is classified into two categories: generalized hereditary peripheral polyneuropathy and generalized acquired peripheral polyneuropathy. Both of these have pathogenic bases or associations with other systemic disorders, including genetic abnormalities. Focal compromises of peripheral nerves are significantly different from generalized processes. They can be secondary to entrapment within a compartment, compression, overuse, transection, or crush due to trauma.

Traumatic peripheral nerve injury is a major cause of severe neural insult which means action potential propagation failure with axonal damage. Traffic accidents are the most common cause of traumatic peripheral nerve injury, but falls or industrial accidents can also lead to peripheral nerve damage (2). The reported incidence of peripheral nerve trauma in the United States is about 45 per 100,000 people per year, similar to that of epilepsy (3). In addition, a retrospective study for patients with both upper and lower limbs trauma has shown that the incidence of

combined peripheral nerve injury was about 1.64%, and it was reported that nerve injuries were particularly common in crush injuries (4). In the upper extremity, the radial, ulnar, and median nerve injuries are common. In the lower extremities, sciatic nerve injuries and peroneal nerve injuries are relatively common, and tibial and femoral injuries are rare (5).

Classification and diagnosis of peripheral nerve injury

Injury of the peripheral nervous system was originally classified by Seddon (6) and Sunderland (7). (Table 1) Neurapraxia is the mildest form of nerve injury with myelin damage; it generally has a good prognosis. Axonotmesis is characterized by axonal loss and Wallerian degeneration, and is caused by transection injury, crush injury, stretch injury, or percussion injury. Sunderland's classification divides Seddon's axonotmesis into three stages based on the level of disruption. Neurotmesis, which generally has the worst prognosis, is a condition in which the nerve tissue is completely damaged and axon regeneration cannot occur. It is very important for clinicians to make an accurate diagnosis of peripheral nerve injury according to the above classification systems in order to make a prognosis and determine the best treatment strategy.

Electrophysiologic studies, including nerve conduction studies (NCS) and needle electromyography (EMG), are the most important tests for the evaluation of peripheral nerve injuries. EMG was the first electrophysiologic technique used to evaluate peripheral neuromuscular disorders; it has since been used as a major

electrodiagnostic tool (8). EMG can detect abnormal membrane potentials of muscle cells, which indicate muscle denervation. Although EMG is currently considered a standard test to evaluate muscle denervation, it has several disadvantages. Its examination procedure is invasive and painful for patients (9). Moreover, it takes time to display abnormalities in the nerve or muscle below the area damaged by peripheral nerve injury (10). Even though the delay depends on the length of nerve segment between the point of injury and testing muscle (11), the evaluation is typically performed approximately 3 weeks after the nerve injury. However, early diagnosis is important because clinical outcomes of peripheral nerve injuries become improved when surgery is performed within a week of injury, and the possibility of recovery declines with increasing delay (12).

In recent decades, the greatest development in the diagnosis and evaluation of peripheral nerve injuries has been the development of radiological examinations. Magnetic resonance imaging (MRI) and ultrasonography (USG) tests can be used to assess not only nerve damage but also surrounding tissue damage. In addition, since the denervated muscle itself may show abnormalities on the MRI or USG test, it may provide additional information over the conventional electrodiagnostic tests (13,14). However, these imaging techniques also have their own disadvantages when evaluating peripheral nerve damage (Table 2).

Investigating molecular changes following muscle denervation as a means of developing a new diagnostic imaging method

As mentioned above, EMG, the current standard test for peripheral nerve injury, has several limitations. Therefore, a new noninvasive functional diagnostic modality would be of great use. To develop this, it may be helpful to look at molecular changes that occur in muscles after denervation, which can be measured through imaging techniques with the appropriate radiotracers.

The nervous system controls peripheral tissue with two mechanisms: the discharge of impulses (neuromotor) and the release of chemicals (neurotrophic). These control mechanisms are responsible for the development and maintenance of skeletal muscle properties. However, if the nervous system is damaged and loses these controls, the skeletal muscles fall into the "denervation" state. Denervation can lead to muscle atrophy as well as alterations in myofibrillar expression, muscle membrane electrical properties, acetylcholine (ACh) sensitivity, and excitation–contraction coupling processes. Historically, there has been disagreement over whether neuromotor or neurotrophic mechanisms have a greater effect on muscle changes after denervation. Recent experimental observations support the view that altered neuromotor activity is the major cause of skeletal muscle dysfunction after denervation rather than neurotrophic factors (15).

Muscle denervation is accompanied by extensive molecular changes that are related to muscle structure, dynamic properties, cell membrane properties, muscle

activation processes, etc. Notably, changes in the expression of cell membrane proteins such as sodium channels cause alterations in the resting membrane potentials of denervated muscle fibers. Following 7-10 days of denervation, the resting membrane potentials approach a depolarized level of -60 mV, which is close to the threshold level needed to produce all-or-none self-sustaining action potentials (16). These are the molecular and electrophysiologic bases of abnormal spontaneous activities (ASA) such as fibrillation potentials and positive sharp waves; these are the strongest evidence for muscle denervation in EMG.

In addition to changes in cell membrane proteins, Behera et al. recently reported increased ^{18}F-fluorodeoxyglucose (FDG) uptake in the denervated muscle from a spared nerve injury model as an incidental finding (17). They had not anticipated this observation, because the purpose of the study was to investigate alterations in ^{18}F-FDG uptake in injured nerves. There have been several studies exploring molecular changes related to glucose metabolism in denervated skeletal muscle. For example, reciprocal glucose transporters (GLUT) -1 and GLUT-4 expression changes after denervation have been demonstrated in previous studies (18,19). However, no studies have clarified the changes in glucose metabolism after skeletal muscle denervation. Therefore, we used a rat complete sciatic transection injury model and confirmed that electrophysiologically verified denervated skeletal muscle showed significantly increased ^{18}F-FDG uptake using positron emission tomography (PET) one week after denervation (20). In addition, we have reported three human cases of increased ^{18}F-FDG uptake in trapezius muscle with spinal accessory neuropathy after head and neck cancer surgery (21). Thus, we have shown that glucose hypermetabolism in denervated skeletal muscle is a robust

physiologic phenomenon.

^{18}F-FDG positron emission tomography as a new functional imaging study to detect muscle denervation

Even though it was deemed possible to develop new noninvasive diagnostic tools for peripheral neuromuscular disorders using visualization of denervated skeletal muscle from ^{18}F-FDG PET scans, further investigation is necessary to evaluate the clinical usefulness of this imaging study. For example, the details of the process, such as the temporal course of glucose hypermetabolism after nerve injury and the relationship between the severity of nerve injury and the signal intensity of ^{18}F-FDG uptake, would be crucial in interpreting changes of muscle signal from PET scans. Pak et al. has shown increased ^{18}F-FDG uptake one week after nerve injury in a complete sciatic nerve injury model in a rat with subsequent gradual decrease in signal intensity (22). However, the acute phase of denervation was not evaluated, and parallel comparisons between EMG and PET were not made. Moreover, the mechanism underlying this phenomenon is still unclear and should be explored.

Thus, the purpose of this study is, first, to examine temporal characteristics of glucose hypermetabolism after muscle denervation, secondly, to investigate the relationship between nerve injury severity and glucose metabolism change through a partial nerve injury model, and thirdly, to elucidate the molecular mechanism of this physiological phenomenon.

Table 1. Classification System for Peripheral Nerve Injury

Seddon classification	Sunderland classification	Pathology	Prognosis
Neurapraxia	Type I	Local myelin injury	Recovery in weeks to months
Axonotmesis	Type II	Disruption of axonal continuity with Wallerian degeneration	Good prognosis with original efferent targets reached
	Type III	Loss of axonal continuity and endoneurial tubes	Poor prognosis and surgery may be required
	Type IV	Loss of axonal continuity, endoneurial tubes, and perineurium	Poor prognosis and surgery necessary
Neurotmesis	Type V	Severance of entire nerve	Prognosis guarded and dependent on nature of injury and local factors

Table 2. Advantages and Disadvantages of Current Diagnostic Methods for Peripheral Nerve Injury

Diagnostic methods		Advantages	Disadvantages
Electrophysiologic study	Nerve conduction study and electromyography	Gold standard Detection of recovery	Invasive, painful Anatomical constraints Limited value at early stage
Imaging study	Ultrasonography	Anatomic context Dynamic image Guidance for other studies	Subjectivity Diminished resolution of deep tissue
	Magnetic resonance imaging	Anatomic context Visualization of nerve regeneration (tractography)	High cost Difficult to predict prognosis

MATERIALS AND METHODS

Animal models

The animal care and experimental procedures followed the protocol approved by the Institutional Animal Care and Use Committee (IACUC) of Seoul National University Hospital (IACUC approval no. 13-0203). Male Sprague-Dawley rats (7 weeks old) were used to create a denervation model. They were anesthetized with isoflurane inhalation and the left sciatic nerve was exposed by splitting the gluteal muscles. For the complete axonal injury model, a nerve segment of length 10 mm was resected just proximal to the bifurcation of the common peroneal and tibial nerves. Sham-operation, exposing the sciatic nerve without resection, was performed on the right side of the rats. For partial axonal injury model, partial ligations of peroneal and tibial divisions of the left sciatic nerve were performed under a microscope. Injury severity was evaluated by NCS. The ratio of compound motor action potential (CMAP) area of the ipsilateral tibialis anterior muscle to that of contralateral tibialis anterior muscle was calculated to quantify peroneal nerve injury. To investigate the role of mechanistic target of rapamycin (mTOR) activity in glucose metabolism in skeletal muscle after denervation, we used rapamycin (mTOR inhibitor) treated rats. Rapamycin (LC Laboratories, Woburn, USA) was initially dissolved in 2% DMSO+30% PEG 300+5% Tween 80+ddH_2O. Rats were injected intraperitoneally with 1 mg/kg/day Rapamycin starting 2 days before the

surgery till 7 days after the surgery. (10 days, total dose of 10 mg/kg). PET scans were performed on the last day.

^{18}F-FDG Positron emission tomography scans

After the surgery, the rats were scanned using a small-animal micro PET/CT system (eXplore VISTA, GE Healthcare). For the PET scan, 37 MBq of ^{18}F-FDG was injected intravenously and animals were kept anesthetized on a warmed platform for 1 hour before imaging. A 20-minute static scan of the hind limbs was obtained. After the PET scan, CT images were obtained. The CT images were used to define the anatomical location of the compartment muscles and the placement of regions of interest (ROIs). The size of the reconstructed voxel was 0.3875 x 0.3875 x 0.675 mm. The ROIs for both sides of the anterolateral and posterior compartment muscles of the lower legs were drawn manually along with the boundary of each compartment. These ROIs were drawn in the axial section, at the mid-lower leg level, which showed prominent ^{18}F-FDG uptake. CT overlay images provided anatomic guidance. To normalize ^{18}F-FDG uptake in the ROIs, we used additional ROIs on both sides of the upper thigh muscles which were not affected by surgery. These were drawn in the axial section and were disk-shaped; the diameters were 7 mm for all ROIs (Fig. 1A). Then we calculated the mean lesion-to-normal counts ratio (LNR_{mean}), defined as the mean count of the ROIs for each compartment divided by the average of the mean counts for both upper thigh ROIs. To examine the temporal characteristics, serial ^{18}F-FDG PET scans and EMG were done 1, 2, and 3 days, and 1, 2, 3, 4, 8, 12, and 19 weeks after the denervation. For

the partial axonal injury model, PET and EMG were done 1 week after the surgery and the results were compared to those of the complete model.

Nerve conduction study and electromyography

Rats were anesthetized for NCS and EMG. A 2-channel portable electrodiagnostic system (Medelec Synergy Plinth, Oxford Instruments, UK) was used for all experiments. CMAPs in gastrocnemius and tibialis anterior muscles were obtained using needle electrodes (Scalp Needle Electrode, Natus Alpine Biomed, Denmark). For EMG, a monopolar electrode (Disposable Monopolar Needles, Natus Neurology, USA) was used to evaluate ASA. Four points in each muscle were measured and ASA was graded 0 to 4: no fibrillation or positive sharp waves at any point is grade 0, fibrillation and positive sharp waves at every point is grade 4.

Histology and molecular studies

After denervation, rats were euthanized in a chamber precharged with carbon dioxide for autopsy. Tissue samples were obtained from both sides of the tibialis anterior muscles. Standard Hematoxylin and Eosin (H&E) stain and immunohistochemistry (IHC) for mononuclear inflammatory cells were performed to rule out the effects of inflammatory reactions one week after denervation. Sections were incubated with rat anti-CD8, rat anti-CD4, rabbit anti-mMBP for eosinophils, or rat anti-F4/80 for macrophages. Inflammatory cell infiltration was quantified by counting the average number of positively stained cells in five

randomly chosen high-power field (HPF, 400x) regions in at least two cross-sections per muscle.

Western blot (WB) analyses were performed to detect protein abundance and protein phosphorylation on days 2 and 7 after denervation. Isolated muscle tissues were homogenized with 350 μl lysis buffer (Pro-Prep protein extract solution, iNtRON biotechnology, Seoul, Korea) on ice. Samples of homogenates were put on ice for at least 1 hour. After 1 hour, they were centrifuged (Microcentrifuge 5424R, Eppendorf, Hamburg, Germany) at 4℃, 15000 rpm, and 30 min for each homogenate sample and the upper solution in each tube was obtained without surface residuals. Bradford assay was used to measure the concentrations of proteins. SDS-PAGE (Mini-PROTEAN, Bio-Rad, Zurich, Switzerland) was used for electrophoresis, followed by transfer to polyvinylidene fluoride (PVDF) membranes using a Mini-PROTEAN apparatus. Then the membranes were blocked for 1 hour at room temperature or overnight at 4℃ with 5% bovine serum albumin (BSA). Primary antibodies used to investigate molecular mechanisms were adenosine monophosphate-activated protein kinase (AMPK), phospho-AMPK, mTOR, phospho-mTOR, phospho-Ca^{2+}/calmodulin-dependent protein kinase II (CaMK II), Bax, and Bcl-2. An antibody against TATA-binding protein (TBP) was used for normalization. Antibodies were purchased from Cell Signaling and Abcam. Optical densities were measured with imaging software (imageJ) for quantification.

Statistical analyses

Wilcoxon signed-rank tests were performed to detect differences in LNR_{mean} from

PET scans and normalized optical density from WB between denervation sides and sham-operation sides. Pearson correlation coefficient was used to evaluate the relationship between ^{18}F-FDG uptake signal and nerve injury severity. A P value of 0.05 was chosen as the level of significance.

RESULTS

Temporal characteristics of glucose metabolism after denervation in skeletal muscle

Serial ^{18}F-FDG PET scans in a complete injury model showed significantly increased ^{18}F-FDG uptake compared to the sham side commencing 2 days after denervation (LNR_{mean}, sham, 1.332 ± 0.205; LNR_{mean}, denervation, 3.151 ± 0.822; n = 5; $P < 0.05$) and continuing for 12 weeks (LNR_{mean}, sham, 1.316 ± 0.275; LNR_{mean}, denervation, 2.661 ± 0.749; n = 5; $P < 0.05$), in anterior compartment muscles, which are innervated by the peroneal division of the sciatic nerve. RM-ANOVA The peak of ^{18}F-FDG uptake appeared one week after denervation(LNR_{mean}, sham, 1.360 ± 0.452; LNR_{mean}, denervation, 10.340 ± 4.094; n = 5; $P < 0.05$). Fibrillation potentials and positive sharp waves in EMG abruptly appeared at 3 days and disappeared 12 weeks after the surgery (Figure 1).

Relationship between nerve injury severity and signal intensity of ^{18}F-FDG uptake

In the partial peroneal injury model, ^{18}F-FDG uptake in the ipsilateral anterolateral compartment was increased compared to that of the sham-operation side after one

week of denervation. However, the increase in ^{18}F-FDG uptake in the partial injury model (LNR_{mean}, partial, 4.119 ± 1.475, n = 6) was less than that of the complete injury model (LNR_{mean}, complete, 10.340 ± 4.094, n = 5). In addition, there was a strong positive correlation between electrophysiologically calculated nerve injury severity and LNR_{mean} (Pearson correlation coefficient 0.63, $P < 0.05$) (Figure 2).

Inflammatory cell infiltration in denervated skeletal muscle

H&E stain of the left tibialis anterior muscle showed no definite change compared to the sham side. As measured by IHC, there was no significantly increased infiltration of inflammatory cells (macrophages, eosinophils, CD4-positive T Cells, or CD8-positive T cells) in denervated muscle compared with the sham side (Figure 3).

Changes in molecular markers related to mTOR activity and apoptosis

Two days after denervation, WB showed that there were no significant changes in expression p-CaMK II, AMPK, p-AMPK, mTOR, p-mTOR, Bcl-2, or Bax. In addition, neither AMPK/mTOR phosphorylation nor apoptotic activity, calculated by the ratio of Bax to Bcl-2, changed significantly. 7 days after denervation, expression of mTOR (sham, 0.103 ± 0.118; denervation, 0.703 ± 0.466, n = 6, $P < 0.05$) and p-mTOR (sham, 0.055 ± 0.0232; denervation, 0.981 ± 0.590, n = 6, P = P

< 0.05) were drastically increased. AMPK (sham, 0.933 ± 0.198; denervation, 2.097 ± 0.493, n = 6, P < 0.05), Bax (sham, 0.358 ± 0.101; denervation, 1.006 ± 0.127, n = 6, P < 0.05), and Bcl-2 (sham, 0.862 ± 0.128; denervation, 1.060 ± 0.062, n = 6, P < 0.05) were also increased. Phosphorylation of mTOR (sham, 0.978 ± 0.692; denervation, 1.520 ± 0.667, n = 6, P = 0.116) increased 7 days after denervation without statistical significance, while that of AMPK (sham, 1.076 ± 0.296; denervation, 0.544 ± 0.348, n = 6, P < 0.05) decreased significantly. The ratio of Bax to Bcl-2 (sham, 0.415 ± 0.100; denervation, 0.947 ± 0.094, n = 6, P < 0.05) increased significantly (Figure 4).

^{18}F-FDG uptake change in denervated skeletal muscle in rapamycin treated rats

One week after complete sciatic transection, rapamycin treated rats also showed increased ^{18}F-FDG uptake in denervated muscle compared to the sham side (LNR_{mean}, sham, 1.348 ± 0.321; LNR_{mean}, denervation, 4.185 ± 1.25; n = 5; P < 0.05). However, it is about 40% of the signal intensity (LNR_{mean}, denervation, rapamycin treated, 4.185 ± 1.253; LNR_{mean}, denervation, rapamycin untrerated, 10.340 ± 4.094; n = 5; P < 0.05) of the untreated complete injury model at the same time point (Figure 5).

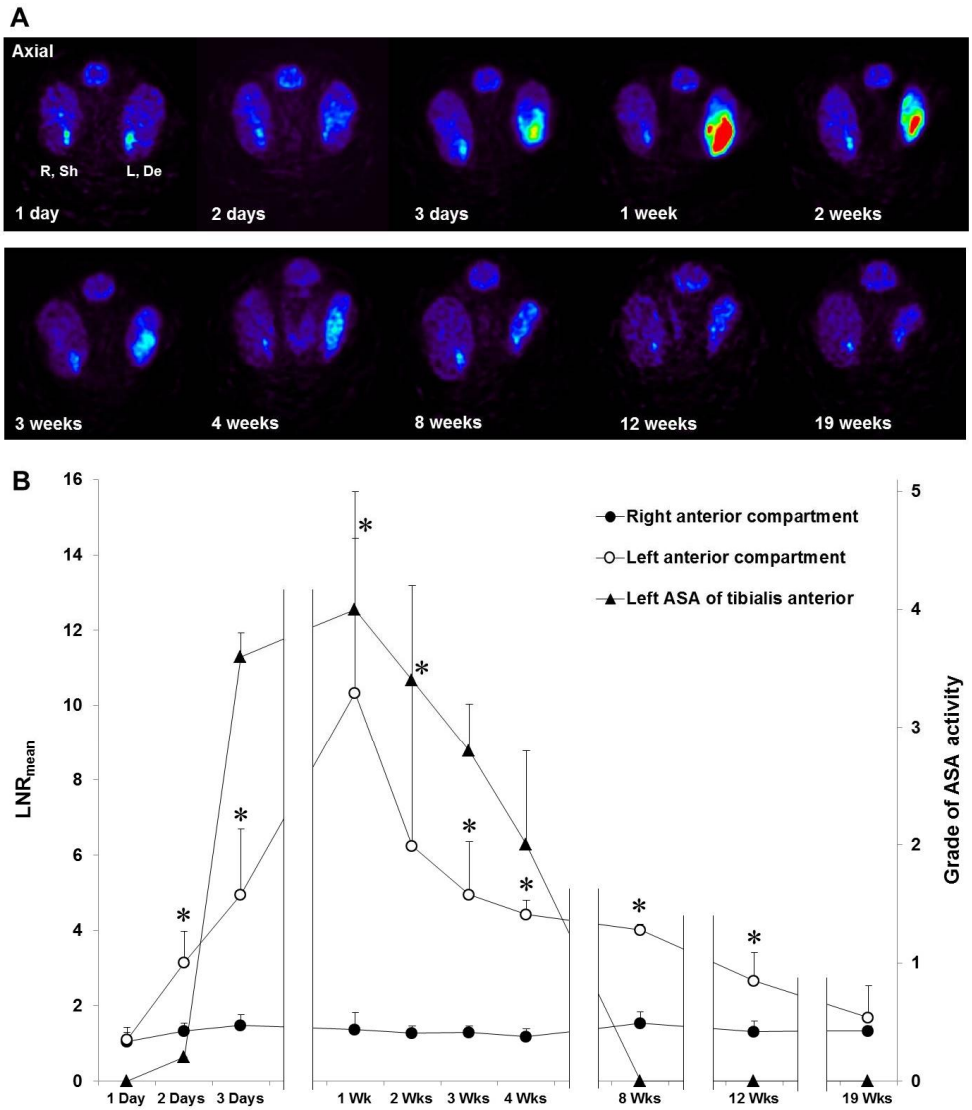

Figure 1. Serial ^{18}F-fluorodeoxyglucose (^{18}F-FDG) positron emission tomography (PET) scans show temporal characteristics of glucose hypermetabolism in denervated skeletal muscle. (A) Axial positron emission tomography (PET) images of the hind limbs were taken 1, 2, and 3 days, and 1, 2, 3, 4, 8, 12, and 19 weeks after denervation. The level of the images was the mid-lower leg and covered both anterior and posterior compartments. Increased ^{18}F-fluorodeoxyglucose (^{18}F-FDG) uptake was observed in both the tibia and fibula

bones. The right side of the image displays denervated lower leg muscles and shows increased ^{18}F-FDG uptake starting 2 days after denervation. Denervation atrophy is observed in serial follow-up. (B) Calculated mean lesion-to-normal counts ratios (LNR_{mean}) from PET scans and graded abnormal spontaneous activities (ASA) from anterior compartment muscle electromyography (EMG) are shown. Significant increase of ^{18}F-FDG uptake began at two days (LNR_{mean}, sham, 1.332 ± 0.205; LNR_{mean}, denervation, 3.151 ± 0.822; n = 5; *P < 0.05) and continued up to twelve weeks (LNR_{mean}, sham, 1.316 ± 0.275; LNR_{mean}, denervation, 2.661 ± 0.749; n = 5; *P < 0.05) after denervation. Alternately, ASA as measured by EMG appeared suddenly on day 3 and disappeared on week 8 after denervation. R, Right; L, Left; Sh, Sham; De, Denervation; Wks, Weeks.

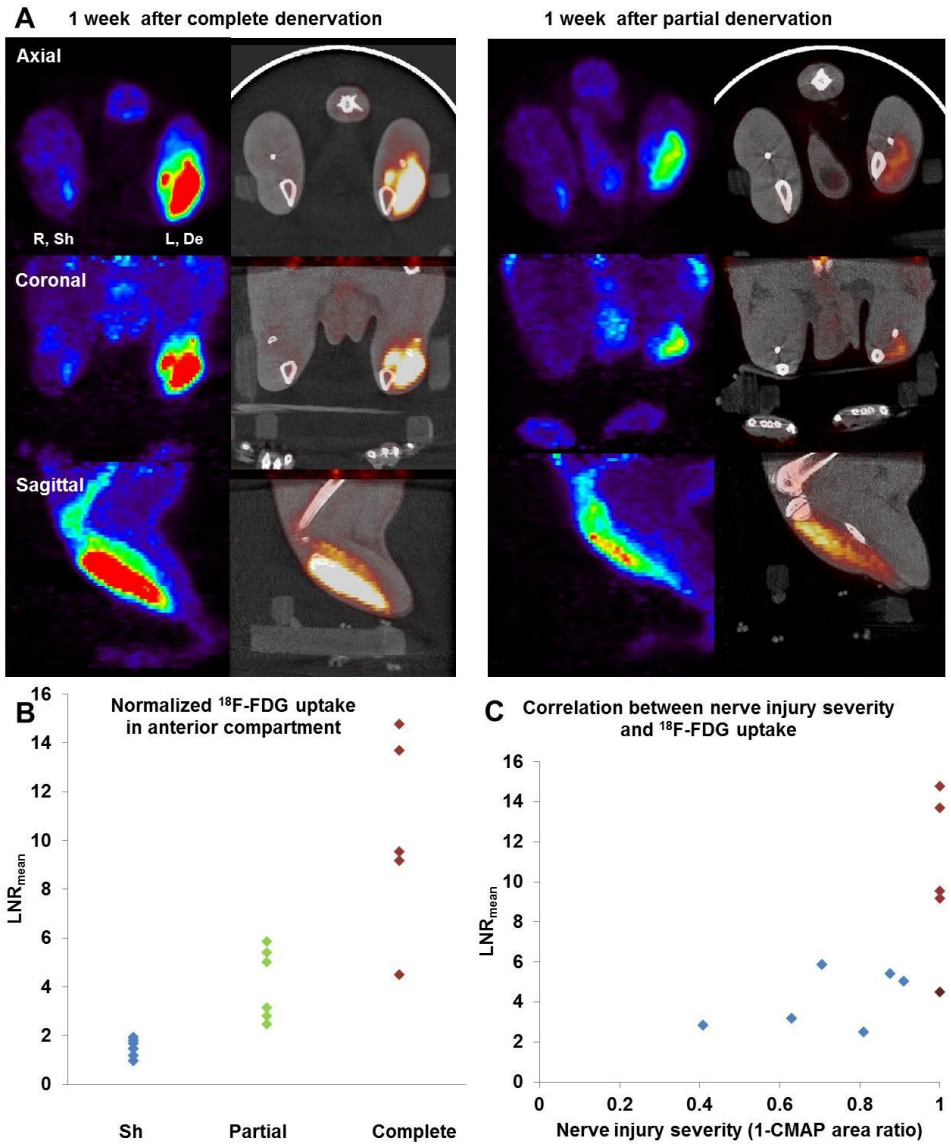

Figure 2. In a partial peroneal injury model, the increase in ^{18}F-FDG uptake is relatively small compared to the increase in ^{18}F-FDG uptake in a complete injury model. (A) ^{18}F-FDG PET scans 1 week after the complete and partial nerve injury model. PET/computed tomography (CT) overlay fusion images are shown on the right side. The increase in ^{18}F-FDG uptake in the partial injury model was less than that of the complete injury model. (B) Calculated LNR_{mean} from PET

scans confirmed moderately increased ^{18}F-FDG uptake (LNR_{mean}, partial, 4.119 ± 1.475, n = 6) in the partial nerve injury model compared to complete injury (LNR_{mean}, complete, 10.340 ± 4.094, n = 5). (C) There was a strong correlation between the severity of nerve injury and the signal intensity of ^{18}F-FDG uptake (Pearson correlation coefficient 0.63, $P < 0.05$). Compound motor action potential (CMAP) area was used to quantify nerve injury severity. R, Right; L, Left; Sh, Sham; De, Denervation.

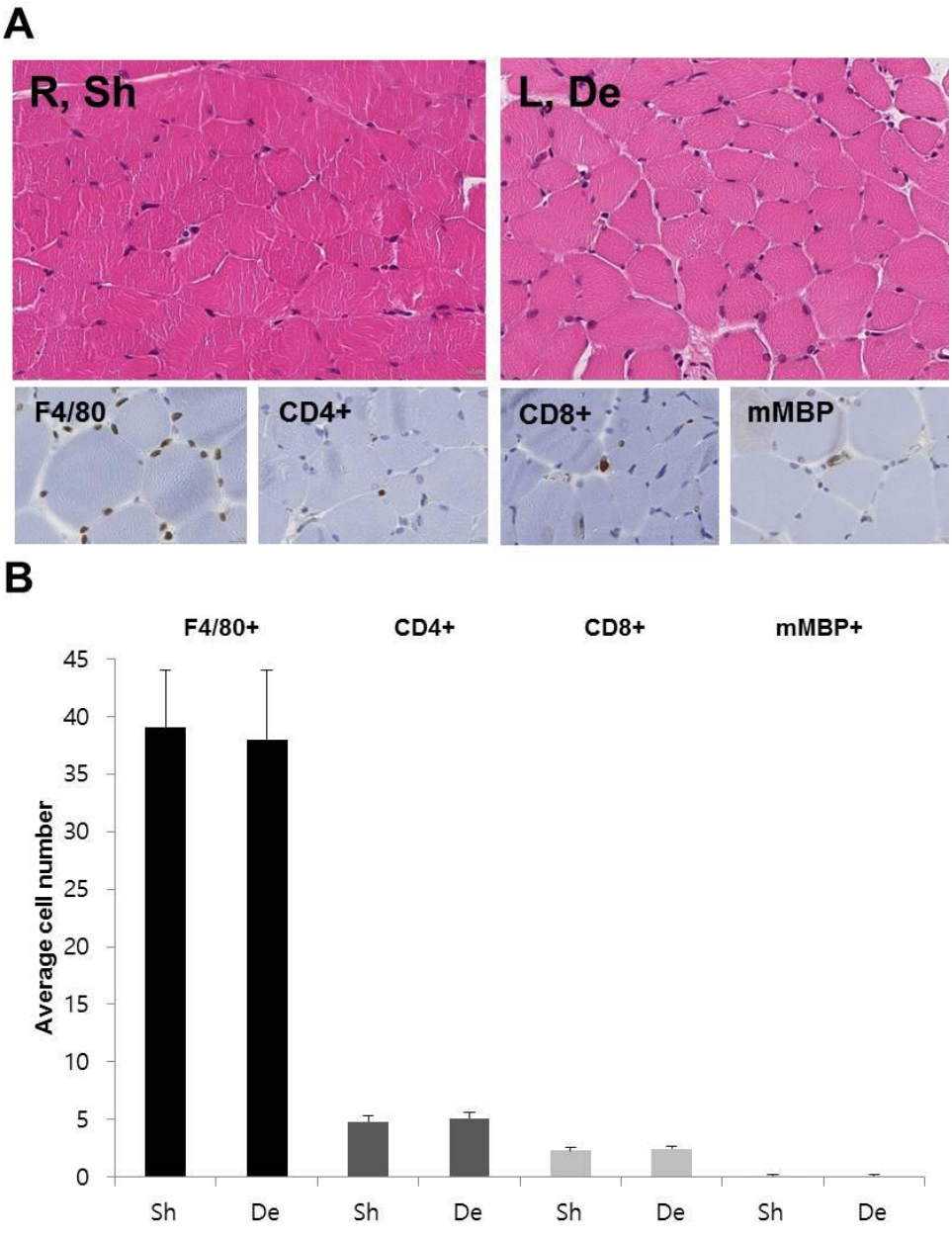

Figure 3. Inflammatory cell infiltration does not increase in the tibialis anterior muscle, one week after denervation. (A) Standard Hematoxylin and Eosin (H&E) stain on the tibialis anterior muscles from both legs showed no definite histologic change. Immunohistochemistry (IHC) labeled inflammatory cells such as macrophages (F4/80), CD4-positive T cells (CD4), CD8-positive T

cells (CD8), and eosinophils (mMBP) in skeletal muscle. (B) Average cell counts for each marker counted in the high-power field (HPF) showed no significant increase in inflammatory cells in the denervated tibialis anterior muscle compared to the sham side. R, Right; L, Left; Sh, Sham; De, Denervation.

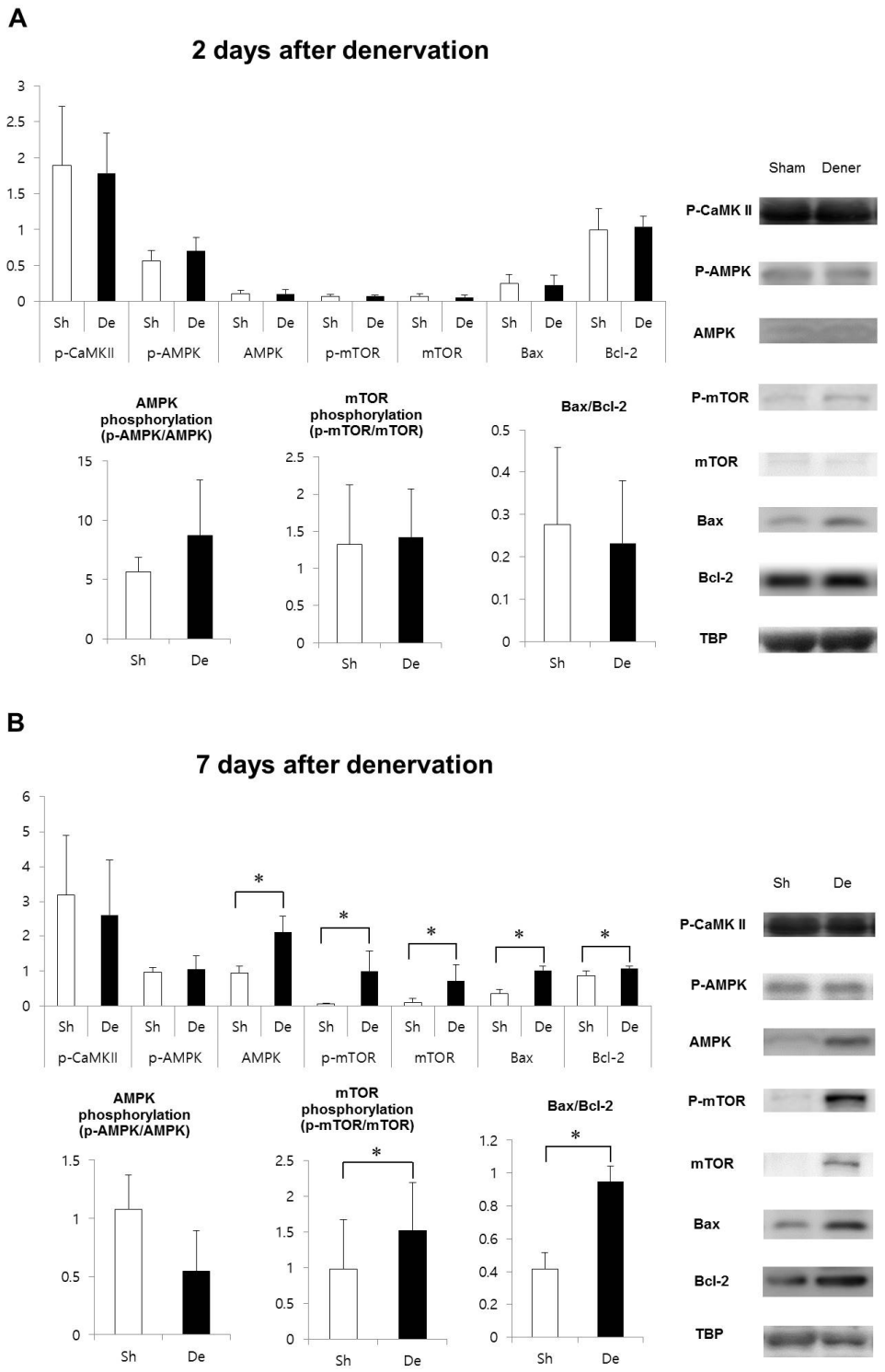

Figure 4. The results from western blot analyses show significantly higher

expressions of proteins related to mTOR and apoptosis pathways in denervated tibialis anterior muscle compared to those in sham side muscle. (A) Two days after denervation, there were no significant changes in the expression of molecular markers related to Ca^{2+}/calmodulin-dependent protein kinase, adenosine monophosphate-activated protein kinase (AMPK), mechanistic target of rapamycin (mTOR), or apoptosis pathways. (B) Significant molecular changes were observed 7 days after denervation. The expression of mTOR (sham, 0.103 ± 0.118; denervation, 0.703 ± 0.466, n = 6, * $P < 0.05$) and phospho-mTOR (p-mTOR, sham, 0.055 ± 0.0232; denervation, 0.981 ± 0.590, n = 6, * $P < 0.05$) increased drastically in denervated tibialis anterior muscle. In addition, the expression of AMPK (sham, 0.933 ± 0.198; denervation, 2.097 ± 0.493, n = 6, * $P < 0.05$), Bax (sham, 0.358 ± 0.101; denervation, 1.006 ± 0.127, n = 6, * $P < 0.05$), and Bcl-2 (sham, 0.862 ± 0.128; denervation, 1.060 ± 0.062, n = 6, * $P < 0.05$) were also increased. Phosphorylation of mTOR (sham, 0.978 ± 0.692; denervation, 1.520 ± 0.667, n = 6, $P = 0.116$) increased without statistical significance, while that of AMPK (sham, 1.076 ± 0.296; denervation, 0.544 ± 0.348, n = 6, * $P < 0.05$) decreased significantly. The ratio of Bax to Bcl-2 (sham, 0.415 ± 0.100; denervation, 0.947 ± 0.094, n = 6, * $P < 0.05$) increased significantly compared to sham side tibialis anterior muscle. Sh, Sham; De, Denervation.

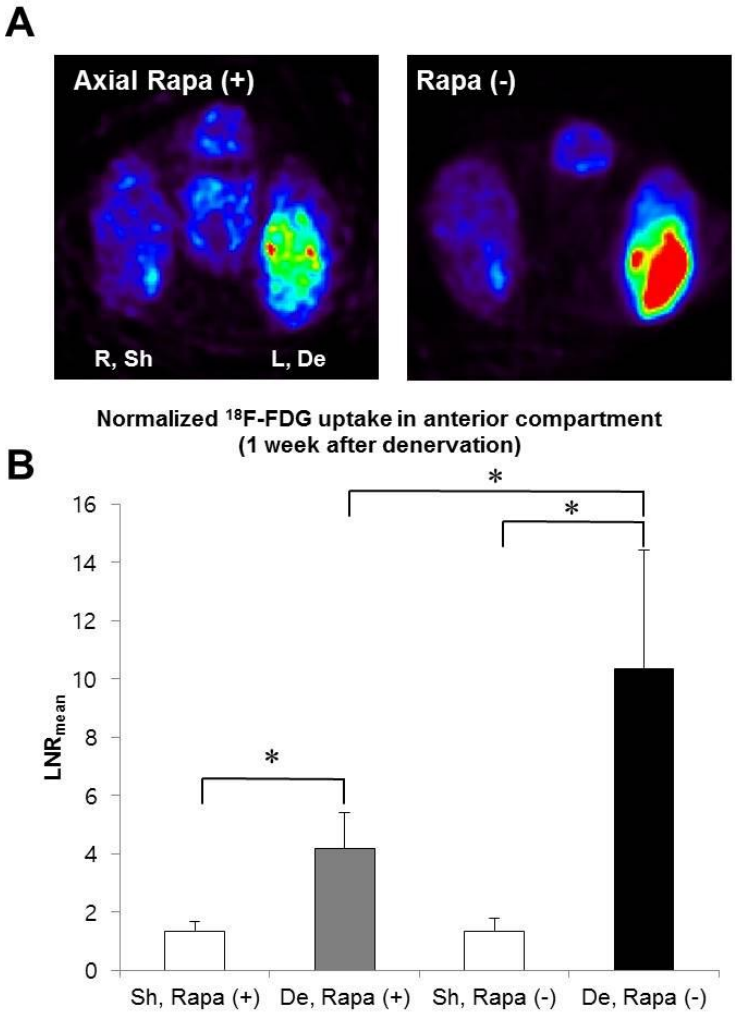

Figure 5. ^{18}F-FDG PET scans of the hind limbs in rapamycin treated rats with left sciatic nerve transection show less increase in ^{18}F-FDG uptake in the denervated muscle compared to the increase in ^{18}F-FDG uptake in untreated rats. (A) Axial PET images of the hind limbs showed increased ^{18}F-FDG uptake in the denervated lower leg muscle of rapamycin-treated rats one week after complete sciatic nerve transection. (B) LNR_{mean} showed the signal intensity in the denervated tibialis anterior muscles of rapamycin-treated rats is about 40% of untreated complete injury rats with statistical significance (LNR_{mean}, denervation, rapamycin

treated, 4.185 ± 1.253; LNR_{mean}, denervation, rapamycin untrerated, 10.340 ± 4.094; n = 5; * $P < 0.05$). R, Right; L, Left; Sh, Sham; De, Denervation; Rapa, Rapamycin.

DISCUSSION

This study has elucidated the temporal characteristics of glucose hypermetabolism in denervated skeletal muscle. It began 2 days after nerve injury and lasted up to 12 weeks, with maximal increase at one week after denervation, in a rat sciatic transection model. There was a strong relationship between nerve injury severity and signal intensity of ^{18}F-FDG from PET scans in our experimental data. In terms of mechanism, this phenomenon seems to involve multiple molecular pathways; among these, mTOR and apoptosis pathways may play critical roles when the ^{18}F-FDG uptake reaches its peak.

One interesting finding regarding temporal characteristics was the observation that metabolic changes in denervated skeletal muscle took place before the development of membrane instability (measured by ASA in EMG) and continued up to the later-measured time points. As mentioned above, electrophysiologic studies are often deferred for up to 3 weeks after nerve injury. However, early detection of peripheral nerve injury is advantageous to optimize functional recovery (23). Our study results imply that ^{18}F-FDG PET scans enable early evaluation of peripheral nerve injury, and the wider time span of metabolic change provides the possibility of developing a new diagnostic tool that overcomes the disadvantages of electrophysiologic studies such as EMG. To model partial nerve injury, we used a method that partially ligates the nerve. Quantification of the degree of nerve injury is possible because the area of CMAP derived from NCS

directly reflects the population of intact axons (24). The results of this study showed that there was a strong correlation between the degree of nerve damage and the strength of the ^{18}F-FDG uptake signal. It implies that the severity of nerve injury can be estimated by interpreting the signal intensity of ^{18}F-FDG PET scans from denervated muscle. However, the temporal characteristics of the signal after nerve injury, as discussed above, must be considered for meaningful estimations.

^{18}F-FDG is the most commonly used radiopharmaceutical for PET studies of cancer and other diseases of the brain and heart (25). Skeletal muscles are not commonly evaluated clinically by ^{18}F-FDG PET scans, but there have been several research studies using ^{18}F-FDG PET in skeletal muscles. One study investigated muscular activity in runners (26) and another study suggested that ^{18}F-FDG PET/CT is potentially useful for identifying dystonic muscles in idiopathic cervical dystonia patients (27). ^{18}F-FDG PET imaging has been proposed as a promising tool for detecting musculoskeletal infection as well (28). Nevertheless, the clinical usefulness of ^{18}F-FDG PET scans in peripheral neuromuscular disorder has not yet been established, except in the treatment of musculoskeletal tumors (29). Moreover, ^{18}F-FDG uptake in muscle has been regarded as a potential source of false-positive readings in PET scanning (30). Our study has successfully elucidated the temporal characteristics of glucose hypermetabolism in denervated muscle after nerve injury as well as the relationship between nerve injury severity and glucose hypermetabolism. Although it is too early to justify the use of ^{18}F-FDG PET scanning to detect and evaluate muscle denervation, the results of this study may suggest a new possible indication for ^{18}F-FDG PET. The experimental data can be

used as reference data to interpret ^{18}F-FDG PET signal intensities in future studies using ^{18}F-FDG PET as a diagnostic tool for peripheral nerve injury. In addition, it is expected that this imaging study might have several advantages, such as early diagnosis and quantification of nerve injury severity, compared to conventional diagnostic tools such as EMG, USG, and MRI. However, there are some disadvantages to be expected. ^{18}F-FDG PET studies present a radiation hazard risk and no particular superiority over other tests in terms of cost. False-positives may appear because glucose hypermetabolism is not a specific physiologic change in muscle denervation. Therefore, further investigation is necessary such as a comparative clinical study between conventional diagnostic modalities and muscle ^{18}F-FDG PET for peripheral nerve injury.

To investigate the mechanism, we first examined the histology of the inflammatory response in denervated muscle, since FDG accumulation can be commonly caused by an inflammatory response (31). Histological changes after denervation can be detected as early as the 7th day in rat sciatic transection models (32). Our H&E stain was compatible with previous results, showing no definite change after denervation. Inflammation can elevate glucose metabolism in tissues (31) and inflammation in skeletal muscle is a common cause of increased ^{18}F-FDG uptake (28). However, our IHC results demonstrated that the inflammatory cell infiltration in denervated skeletal muscle is not increased compared to the sham side one week after denervation. Unlike in inflammatory myopathy, the role of inflammation is not prominent in denervation atrophy (1). This means that hypermetabolism in denervated muscle is likely not attributed to the influence of

inflammation.

One possible mechanism of glucose hypermetabolism is spontaneous muscle contraction after nerve injury. In 1964, Bowman and Raper proposed that there was a connection between the membrane potential and carbohydrate metabolism in skeletal muscle (33). In fact, fibrillation potential is considered a spontaneous and uncoordinated activity of muscle fiber and can even be seen by the naked eye or on ultrasound examination (34). Because increased muscular activity is associated with an increase in glucose metabolism (26), abundant fibrillation may be triggering the abrupt increase in ^{18}F-FDG uptake. Our experimental results reveal similar temporal courses between ^{18}F-FDG uptake and membrane instability measured with EMG. Both show the peak value at one week after denervation. These findings also imply that glucose hypermetabolism is affected by fibrillation potential in spite of the sudden appearance of fibrillation 3 days after nerve injury. Contracting skeletal muscle increases glucose uptake via the AMPK pathway, and calcium-sensitive pathway (CaMK) (35–37). Both pathways activate their downstream effectors, increase expression of GLUT4, and translocate it into the cell membrane (35,38–40). However, the mechanism underlying glucose uptake increase in denervated muscle could be different from the metabolic process in normal skeletal muscle. For example, the recruitment of GLUT to increase glucose uptake in denervated muscle, as mentioned above, is different from normal contracting muscle (18–20). Our WB results support these conclusions. Even though the expression of AMPK increased 7 days after denervation, AMPK phosphorylation significantly decreased in denervated muscle compared to the

sham side. In addition, there was no significant expression change in p-CaMK II after denervation. Therefore, the glucose uptake increase in denervated muscle may not be mediated by the AMPK and calcium-sensitive pathways.

Muscle denervation is a complicated process and several important molecular pathways involved in denervation might be related to glucose metabolism. The mTOR pathway is one possibility, and while it is generally considered to be an important component of cell growth and proliferation, it also plays a role in the atrophy of muscles after denervation (41,42). Glucose transport is regulated by the mTOR pathway as well (43). Although our results showed that there was no statistically significant increase in the phosphorylation of mTOR, p-mTOR and mTOR expression increased most prominently at the peak of ^{18}F-FDG uptake. The results of PET scans from rats treated with rapamycin, an mTOR inhibitor, were fascinating and confirmed the role of the mTOR pathway. The result suggests that at least half of the increase in ^{18}F-FDG uptake at the peak of glucose hypermetabolism in muscle denervation was due to the mTOR pathway. Even though this result is strong evidence for the association between mTOR and glucose hypermetabolism in muscle denervation, it does not guarantee a direct link between the two. Several other molecular pathways, such as the ubiquitin-proteasome pathway, are associated with mTOR pathways (48,49), and are involved in regulation of net protein balance during denervation processes.

Another possible hypothesis involves an apoptotic reaction in denervated

skeletal muscle. Apoptosis has been considered an energy consuming process that can be accompanied by FDG uptake increase (44,45). There are several previous studies demonstrating that muscle denervation stimulates mitochondria-mediated apoptosis (46,47). With respect to apoptosis, the expression of Bax and Bcl-2, and the ratio of apoptotic activity (Bax/Bcl-2) increased significantly 7 days after denervation. These results indicate that apoptosis had already begun at this point and it can affect increased glucose metabolism.

There were no significant changes in the expression of CaMK, mTOR, AMPK, or apoptotic pathway proteins 2 days after denervation. At that time, glucose metabolism increased significantly without ASA. It means that none of the molecular pathways we have examined can explain increased glucose hypermetabolism in early stage muscle denervation. Thus, the mechanism is most likely heterogeneous and multiphasic during the whole denervation process. Further study is necessary to elucidate the precise molecular mechanisms.

There were several limitations to our study. Five rats per group were used for ^{18}F-FDG PET scans and six rats per group for molecular experiments. A larger number of rats would be needed to gain stronger evidence, especially for the partial nerve injury study. Moreover, the term "partial nerve injury" is not clearly defined, and can occur in a variety of forms depending on the mechanism of injury. For example, transient nerve compression with lower pressure causes a demyelinating lesion without definite Wallerian degeneration (50). Therefore, many animal peripheral

nerve injury models have been developed to reflect various clinical situations (50–53). Our partial nerve injury model is considered a “partial neurotmesis” model, and our study does not cover the glucose metabolism characteristics of muscles in other forms of partial nerve injuries. The grading system for ASA in EMG studies also has potential problems. It is similar to the grading system for clinical EMG studies in humans (1), which can be subjective and arbitrary. Quantification of ASA is very difficult, and is one of the major disadvantages of EMG. In serial follow-up experiments, we had to divide the ^{18}F-FDG PET group (n = 5) and EMG group (n = 5) because needle EMG is an invasive procedure which can alter ^{18}F-FDG uptake signal in denervated muscle through inflammatory response. Thus, direct comparison between serial ^{18}F-FDG PET results and EMG results was not feasible. For the rapamycin study, we could not conduct EMG in rapamycin treated rats. If we were able to observe the associations between ^{18}F-FDG PET and EMG studies in rapamycin-treated denervation animals, we could have learned more about mTOR's contribution to the mechanism underlying glucose metabolism.

In conclusion, glucose hypermetabolism in denervated muscle is a peculiar phenomenon and has several characteristics related to temporal course and peripheral nerve injury severity. Our study results suggest that ^{18}F-FDG PET scans may one day be used to develop a new functional imaging study for the diagnosis and evaluation of peripheral nerve injury. With this imaging study, quantification of nerve injury and early diagnosis of muscle denervation might be possible. The underlying molecular mechanism is most likely heterogeneous and multiphasic during the atrophy process; however, the mTOR pathway plays an important role,

especially when glucose metabolism is at its peak.

REFERENCES

1. Amato A, Dumitru D. Electrodiagnostic medicine. 2nd Ed. Elsevier; 2002

2. Robinson LR. Traumatic injury to peripheral nerves. Muscle Nerve. 2000;23(6):863–73.

3. Kurtzke JF. The current neurologic burden of illness and injury in the United States. Neurology. 1982;32(11):1207–14.

4. Taylor CA, Braza D, Rice JB, Dillingham T. The Incidence of Peripheral Nerve Injury in Extremity Trauma. Am J Phys Med Rehabil. 2008;87(5).

5. Noble J, Munro CA, Prasad VS, Midha R. Analysis of upper and lower extremity peripheral nerve injuries in a population of patients with multiple injuries. J Trauma. 1998;45(1):116–22.

6. Seddon HJ. Surgical disorders of the peripheral nerves. 2nd Ed. New york: Churchill Livingstone; 1975. p.21-23.

7. Sunderland S. Nerves and nerve injuries. 2nd Ed. New york: Churchill Livingstone; 1978. p.133-138.

8. Daube JR, Rubin DI. Needle electromyography. Muscle Nerve. 2009 Feb;39(2):244–70.

9. Moon Y-E, Kim S-H, Choi W-H. Comparison of the effects of vapocoolant spray and topical anesthetic cream on pain during needle electromyography in the medial gastrocnemius. Arch Phys Med Rehabil. 2013 May ;94(5):919–24.

10. Buchthal F, Rosenfalck P. Spontaneous electrical activity of human muscle.

Electroencephalogr Clin Neurophysiol. 1966 Apr;20(4):321–36.

11. Thesleff S. Physiological effects of denervation of muscle. Ann N Y Acad Sci. 1974;228(1):89–104.

12. R B. Surgical disorders of the peripheral nerves. 2nd ed. London: Springer; 2011.p.375–428.

13. Wessig C, Koltzenburg M, Reiners K, Solymosi L, Bendszus M. Muscle magnetic resonance imaging of denervation and reinnervation: correlation with electrophysiology and histology. Exp Neurol. 2004 Feb ;185(2):254–61.

14. Simon NG, Ralph JW, Lomen-Hoerth C, Poncelet AN, Vucic S, Kiernan MC, et al. Quantitative ultrasound of denervated hand muscles. Muscle and Nerve. 2015;52(2):221–30.

15. Midrio M. The denervated muscle: facts and hypotheses. A historical review. Eur J Appl Physiol. 2006 Sep ;98(1):1–21.

16. Thesleff S, Ward MR. Studies on the mechanism of fibrillation potentials in denervated muscle. J Physiol. 1975;244(2):313–23.

17. Behera D, Jacobs KE, Behera S, Rosenberg J, Biswal S. ^{18}F-FDG PET/MRI can be used to identify injured peripheral nerves in a model of neuropathic pain. J Nucl Med . 2011 Aug;52(8):1308–12.

18. Castelló a, Cadefau J, Cussó R, Testar X, Hesketh JE, Palacín M, et al. GLUT-4 and GLUT-1 glucose transporter expression is differentially regulated by contractile activity in skeletal muscle. J Biol Chem. 1993 Jul 15;268(20):14998–5003.

19. Handberg A, Megeney LA, McCullagh KJ, Kayser L, Han XX, Bonen A.

Reciprocal GLUT-1 and GLUT-4 expression and glucose transport in denervated muscles. Am J Physiol Endocrinol Metab. 1996 Jul;271(1):50-57.

20. Lee SH, Oh B-M, Lee G, Choi H, Cheon GJ, Lee S-U. Feasibility of ^{18}F-FDG PET as a Noninvasive Diagnostic Tool of Muscle Denervation: A Preliminary Study. J Nucl Med. 2014;55:1737–40.

21. Lee SH, Seo HG, Oh B-M, Choi H, Cheon GJ, Lee S-U. Increased ^{18}F-FDG uptake in the trapezius muscle in patients with spinal accessory neuropathy. J Neurol Sci. 2016;362:127–30.

22. Pak K, Shin MJ, Hwang S-J, Shin J-H, Shin HK, Kim SJ, et al. Longitudinal Changes in Glucose Metabolism of Denervated Muscle after Complete Peripheral Nerve Injury. Mol Imaging Biol. 2016;18(5):741–7.

23. Simon NG, Spinner RJ, Kline DG, Kliot M. Advances in the neurological and neurosurgical management of peripheral nerve trauma. J Neurol Neurosurg Psychiatry.2016;87(2):198–208.

24. David C. Preston BES. Electromyography and neuromuscular disorders. 2nd Ed. Elsevier Health Sciences; 2012.

25. Fletcher JW, Djulbegovic B, Soares HP, Siegel B a, Lowe VJ, Lyman GH, et al. Recommendations on the use of ^{18}F-FDG PET in oncology. J Nucl Med. 2008 Mar;49(3):480–508.

26. Tashiro M, Fujimoto T, Itoh M, Kubota K, Fujiwara T, Miyake M, et al. ^{18}F-FDG PET imaging of muscle activity in runners. J Nucl Med. 1999 Jan;40(1):70–6

27. Sung DH, Choi JY, Kim D-H, Kim E-S, Son Y-I, Cho Y-S, et al. Localization of dystonic muscles with ^{18}F-FDG PET/CT in idiopathic cervical dystonia. J Nucl

Med. 2007 Nov;48(11):1790–5.

28. Strobel K, Stumpe KDM. PET/CT in musculoskeletal infection. Semin Musculoskelet Radiol. 2007 Dec;11(4):353–64.

29. Aoki J, Endo K, Watanabe H, Shinozaki T, Yanagawa T, Ahmed AR, et al. FDG-PET for evaluating musculoskeletal tumors: a review. J Orthop Sci. 2003 Jan;8(3):435–41.

30. Yeung HWD, Grewal RK, Gonen M, Schoder H, Larson SM. Patterns of ^{18}F-FDG Uptake in Adipose Tissue and Muscle: A Potential Source of False-Positives for PET. J Nucl Med. 2003 Nov 1;44(11):1789–96.

31. Mochizuki T, Tsukamoto E, Kuge Y, Kanegae K, Zhao S, Hikosaka K, et al. FDG uptake and glucose transporter subtype expressions in experimental tumor and inflammation models. J Nucl Med. 2001;42(10):1551–5.

32. Pellegrino C, Franzini C. an Electron Microscope Study of Denervation Atrophy in Red and White Skeletal Muscle Fibers. J Cell Biol. 1963;17(2):327–49.

33. Bowman WC, Raper C. Spontaneous fibrillary activity of denervated muscle. Nature. 1964 Jan 11;201:160–2.

34. Pillen S, Nienhuis M, van Dijk JP, Arts IMP, van Alfen N, Zwarts MJ. Muscles alive: ultrasound detects fibrillations. Clin Neurophysiol. 2009 May;120(5):932–6

35. Jørgensen SB, Richter EA, Wojtaszewski JFP. Role of AMPK in skeletal muscle metabolic regulation and adaptation in relation to exercise. J Physiol. 2006;574(1):17–31.

36. Wright DC, Hucker KA, Holloszy JO, Han DH. Ca2+ and AMPK Both Mediate Stimulation of Glucose Transport by Muscle Contractions. Diabetes. 2004 Jan

27;53(2):330 LP-335.

37. Jensen TE, Rose AJ, Jørgensen SB, Brandt N, Schjerling P, Wojtaszewski JFP, et al. Possible CaMKK-dependent regulation of AMPK phosphorylation and glucose uptake at the onset of mild tetanic skeletal muscle contraction. Am J Physiol - Endocrinol Metab. 2007 Apr 27;292(5):1308 -1317.

38. Jessen N, Goodyear LJ. Contraction signaling to glucose transport in skeletal muscle. J Appl Physiol. 2005 Jun 21;99(1):330-337.

39. Rose AJ, Richter EA. Skeletal Muscle Glucose Uptake During Exercise: How is it Regulated? Physiology. 2005 Jul 14;20(4):260–70.

40. Ojuka EO, Goyaram V, Smith JAH. The role of CaMKII in regulating GLUT4 expression in skeletal muscle. Am J Physiol - Endocrinol Metab. 2012 Aug 1;303(3):322 -331.

41. Machida M, Takeda K, Yokono H, Ikemune S, Taniguchi Y, Kiyosawa H, et al. Reduction of ribosome biogenesis with activation of the mTOR pathway in denervated atrophic muscle. J Cell Physiol. 2012;227(4):1569–76.

42. Argadine HM, Mantilla CB, Zhan W-Z, Sieck GC. Intracellular signaling pathways regulating net protein balance following diaphragm muscle denervation. Am J Physiol Cell Physiol. 2011 Feb;300(2):318-27.

43. Buller CL, Loberg RD, Fan M-H, Zhu Q, Park JL, Vesely E, et al. A GSK-3/TSC2/mTOR pathway regulates glucose uptake and GLUT1 glucose transporter expression. Am J Physiol - Cell Physiol. 2008;295(3):836-43.

44. Haberkorn U, Bellemann ME, Brix G, Kamencic H, Morr I, Traut U, et al. Apoptosis and changes in glucose transport early after treatment of Morris

hepatoma with gemcitabine. Eur J Nucl Med Mol Imaging . 2001 Apr ;28(4):418–25.

45. Furuta M, Hasegawa M, Hayakawa K, Yamakawa M, Ishikawa H, Nonaka T, et al. Rapid rise in FDG uptake in an irradiated human tumour xenograft. Eur J Nucl Med. 1997 Apr;24(4):435–8

46. Adhihetty PJ, O'Leary MFN, Chabi B, Wicks KL, Hood DA. Effect of denervation on mitochondrially mediated apoptosis in skeletal muscle. J Appl Physiol. 2007 Mar;102(3):1143–51.

47. Muller FL, Song W, Jang YC, Liu Y, Sabia M, Richardson A, et al. Denervation-induced skeletal muscle atrophy is associated with increased mitochondrial ROS production. Am J Physiol Regul Integr Comp Physiol. 2007 Sep;293(3):1159-68

48. Quy PN, Kuma A, Pierres P, Mizushima N. Proteasome-dependent activation of mammalian target of rapamycin complex 1 (mTORC1) is essential for autophagy suppression and muscle remodeling following denervation. J Biol Chem. 2013;288(2):1125–34.

49. Kelleher AR, Pereira SL, Jefferson LS, Kimball SR. REDD2 expression in rat skeletal muscle correlates with nutrient-induced activation of mTORC1: responses to aging, immobilization, and remobilization. Am J Physiol Endocrinol Metab. 2015;308(2):122-9.

50. Lim J-Y, Cho S-H, Han TR, Paik N-J. Dose-Responsiveness of Electrophysiologic Change in a New Model of Acute Carpal Tunnel Syndrome. Clin Orthop Relat Res.2004;427(427):120–6.

51. Decosterd I, Woolf CJ. Spared nerve injury: An animal model of persistent peripheral neuropathic pain. Pain. 2000;87(2):149–58.

52. Selzer Z, Dudner R, Shir Y. A novel behavioral model of neuropathic pain disorders produced in rats by partial sciatic nerve injury. Pain. 1990;43:205–18.

53. Ho Kim S, Mo Chung J. An experimental model for peripheral neuropathy produced by segmental spinal nerve ligation in the rat. Pain. 1992;50(3):355–63.

국문초록

말초신경의 손상은 외상을 포함한 각종원인에 의해 발생하며, 이로 인해 그 신경이 지배하는 근육의 탈신경을 일으킨다. 탈신경된 근육은 시간이 지남에 따라 분자적 수준에서 다양한 변화가 나타난다. 그 중에서도 포도당 대사가 항진되는 현상이 동물실험에서 플루오르데옥시글루코스를 이용한 양전자 단층촬영 기법을 통해 보고된 바 있고, 실제 사람에서 같은 현상이 확인된 바 있다. 본 연구의 목적은 이러한 탈신경 근육의 포도당 대사증진 현상의 특성을 살펴보고, 또한 그 분자적 기전을 탐색하여 임상적 활용의 토대를 마련하고자 한다.

백서에서 좌골신경을 절단하여 완전신경손상과 좌골신경 지배 근육의 탈신경을 일으키고, 이후 플루오르데옥시글루코스 양전자단층촬영을 백서의 하지에서 연속적으로 촬영하여 포도당 대사 증진의 시간적 특성을 살펴보았다. 또한 좌골신경의 비골분지를 부분적으로 결찰하여 부분신경손상을 일으킨 후, 신경전도검사를 통해 신경손상의 정도를 정량화하였다. 이후 양전자단층촬영을 시행하여 플루오르데옥시글루코스 섭취의 증가를 측정하여 신경전도검사의 결과와 비교를 통해 탈신경 근육에서 신경손상 정도와 포도당 대사항진 간의 상관관계를 조사하였다. 마지막으로 포도당 대사와 관련된 몇 가지 세포 내 경로의 중요 분자

표지자들의 발현을 웨스턴 블롯을 통해 살펴보고, 특히 mTOR (mechanistic target of rapamycin)억제제인 라파마이신을 투여한 쥐에서 탈신경근육의 포도당 대사 변화를 확인해 mTOR 경로가 본 현상에 미치는 영향을 확인하였다.

연구결과 탈신경 근육의 포도당 대사 증진은 백서의 좌골신경 완전손상 모델에서 신경손상 2일째부터 (LNR_{mean}, sham, 1.332 ± 0.205; LNR_{mean}, denervation, 3.151 ± 0.822; n = 5; P < 0.05) 유의미한 플루오르데옥시글루코스의 섭취 증가가 나타났고 12주까지 (LNR_{mean}, sham, 1.316 ± 0.275; LNR_{mean}, denervation, 2.661 ± 0.749; n = 5; P < 0.05) 지속되었다. 그리고 신경손상 1주일 째 가장수술을 시행한 측과 비교하여 7배 이상의 최대섭취증가가 나타났다. (LNR_{mean}, sham, 1.360 ± 0.452; LNR_{mean}, denervation, 10.340 ± 4.094; n = 5; P < 0.05) 부분신경손상 동물모델에서는 완전신경손상에 비해 섭취가 감소되었으며, 정량화된 신경손상의 정도와 플루오르데옥시글루코스 섭취 신호와는 강한 상관관계를 보였다. (Pearson correlation coefficient 0.63, p<0.05). 신경손상 1주일 째 얻은 탈신경 근육조직에서 시행한 웨스턴 블롯 검사에서 mTOR (sham, 0.103 ± 0.118; denervation, 0.703 ± 0.466, n = 6, P < 0.05), p-mTOR (sham, 0.055 ± 0.0232; denervation, 0.981 ± 0.590, n = 6, P < 0.05), Bax (sham, 0.358 ± 0.101; denervation, 1.006 ± 0.127, n = 6, P < 0.05), 및 bcl-2 (sham, 0.862 ± 0.128; denervation, 1.060 ± 0.062, n = 6, P < 0.05)에서 유의미한 발현증가를 보였다. 또한 라파마이신을 투여한 백서에서 좌골신경 손상

후 1주일 째 시행한 양전자단층촬영 검사에서는 데옥시글루코스의 섭취가 증가하였으나, 라파마이신을 투여하지 않은 완전신경손상 백서에 측정된 신호강도에 비해 40% 가량으로 줄어든 결과를 보였다. (LNR_{mean}, denervation, rapamycin treated, 4.185 ± 1.253; LNR_{mean}, denervation, rapamycin untrerated, 10.340 ± 4.094; $n = 5$; $P < 0.05$)

탈신경 근육의 포도당대사 증진 현상은 백서 모델에서 신경손상 이후 2일째 시작되어 1주째 최대가 되는 특성을 가지고 있으며, 증가된 포도당 섭취의 정도는 신경손상의 정도와 관련성을 가지고 있다. 이 현상은 분자수준에서 다양한 신호경로가 관여하고, 시기에 따라 주된 경로가 다를 것으로 생각되며, mTOR 경로가 특히 최대섭취시기에 중요한 역할을 하는 것으로 생각된다. 본 연구의 결과는 말초신경손상의 진단 및 평가를 위한 새로운 기능적 영상검사법 개발에 활용될 수 있을 것으로 기대된다.

색인 : 말초신경손상, 탈신경 근육, 포도당 대사, 플루오르데옥시글루코스, 양전자단층촬영, mTOR

학번 : 2013-21688